COMMUNICATION

Design of a dual Ir-Eu tag for fluorescent visualization and ICP-MS quantification of SIRPα and its host cells

Chunlan Liu[1,2] · Pengtao Li[3] · Xiaowen Yan[1] · Limin Yang[1] · Pingguo Liu[3] · Qiuquan Wang[1]

Abstract

With the expansion of ICP-MS application into the field of bioanalysis, there is an urgent need for novel element tags today. Here, we report the design of a dual-element Ir-Eu tag, opening the door to simultaneous fluorescent imaging and ICP-MS quantification. The ratio of ^{153}Eu/^{193}Ir may serve as a precision control of the labeling process, allowing internal validation of the quantitative results obtained. As for SIRPα and its host cell analysis exemplified here, the Ir-Eu tag demonstrated superior figures of ICP-MS quantification with the LOD (3σ) down to 0.5 (^{153}Eu) and 1.1 (^{193}Ir) pM SIRPα and 220 (^{153}Eu) and 830 (^{193}Ir) RAW264.7 cells more than 130 times more sensitive compared with the LOD (3σ) of 65.2 pM SIRPα at 612 nm using fluorometry. Not limited to these demonstrations, we believe that the design ideas of the dual Ir-Eu tags should be applicable to various cases of bioanalysis when dual optical profiling and ICP-MS quantification are indispensable.

Keywords ICP-MS · Fluorescent imaging · Dual-element tag · SIRPα · Cell

Introduction

So far fluorometry and mass spectrometry have been recognized as two of the main tools for bioanalysis. Moreover, the synergistic use of them should be a more powerful strategy for easily optic-profiling and accurately quantifying biomolecules and/or their host cells in complex biological samples, providing more comprehensive information of targeted bioanalytes. Although some targeted analytes could be directly detected, a consensus has been reached within chemical measurement science community that many of them should be labeled first with suitable optical and/or mass tags for improving not only sensitivity but also selectivity [1]. This is almost a prerequisite especially when inductively coupled plasma mass spectrometry (ICP-MS) is applied for quantification, in which the m/z of labeled element/isotope ions is determined to reflect the content of the targeted bioanalytes [1–4]. In such a circumstance, both stable and sensitive optical and m/z signals simultaneously from the same tag itself are much more desired [5, 6] rather than, respectively, from different tags [7–9], launching the development of an expanded element-tag toolbox that can be more efficiently used for not only optical spectrometric but also ICP-MS bioanalysis. Fortunately, lanthanides (Ln) have very charming fluorescent properties of stable and sharp signals with millisecond lifetime ranging from the visible (for example, Eu and Tb) to near-infrared (Yb, Er, Nd) region because the inner-shell 4f-4f transitions of the Ln are formally parity forbidden [10, 11]. More importantly, on the other hand, all the Ln are very sensitive on ICP-MS [12, 13] due to their relatively low first ionization potentials of around 5.5 eV

Chunlan Liu and Pengtao Li have equal contribution.

✉ Pingguo Liu
  pgliu@xmu.edu.cn

✉ Qiuquan Wang
  qqwang@xmu.edu.cn

1   Department of Chemistry & the MOE Key Laboratory of Spectrochemical Analysis and Instrumentation, College of Chemistry and Chemical Engineering, Xiamen University, Xiamen 361005, China

2   College of Chemistry and Bioengineering, Yichun University, Yichun 336000, China

3   Department of Hepatobiliary Surgery & Fujian Provincial Key Laboratory of Chronic Liver Disease and Hepatocellular Carcinoma, Xiamen Key Laboratory of Translational Medical of Digestive System Tumor, Zhongshan Hospital of Xiamen University, School of Medicine, Xiamen University, Xiamen 361000, China

[14], thus a high ionization efficiency in Ar (15.8 eV)-based ICP. Therefore, dual fluorescent and ICP-MS signals can be simultaneously obtained from the same Ln element through sophisticated molecular design. However, it should be noted that Ln do not have high enough molar absorption coefficient mainly because of their small light-absorbed diameters. An energy antenna moiety as the donor sensitizer for Ln-cored complex chromophores must be employed, which can absorb energy and then transfer to the Ln-cored complex via a rapid internal conversion process for pumping the Ln to excited states [6, 11]. Rational selection of the light-antenna sensitizers is very important to match the energy-requested by the Ln used that emit light signals at their characteristic wavelength. Previous studies showed that a luminescent organometallic complex compared with the conventional organic dyes has many desirable properties for the use as a light-antenna that transfers energy to the Ln [15]. The advantages include the intense light absorption and long-lived excited states with a triplet metal-to-ligand charge-transfer character, thus maximizing the likelihood of energy transfer to the Ln-complex, and photochemical stability and kinetic inertness as well as luminescence of their own, not only providing a basis to monitor energy transfer to the Ln acceptor [16], but also, more meaningfully, offering another ICP-MS signal source along with the Ln when they conjugate with each other to form a dual-element tag, thus resulting in a precision control for a more accurate analysis. Among numerous fluorescent organometallic complexes, the Ir-cored complex formed between Ir(III) and phenylpyridine-type ligands should be a judicious choice as a light-antenna for the Ln-cored complexes due to the fact that its characteristic excited-state energies are well more than 19 000 cm^{-1} over that of, for example, Eu ($^5D_0$, 17,200 cm^{-1}) [17, 18].

Here, we design and synthesize a series of dual Ir-Eu tags with Ir and/or Eu fluorescent and ICP-MS signals by linking Eu-DOTA (DOTA stands for 1,4,7,10-tetraazacyclodo-decane-1,4,7,10-tetraacetic acid) and DCBP-Ir-APP (DCBP stands for 6, 6′-dichloro-3, 3′-bipyridine and APP 4-amino-7H-pyrrole pyrimidine) with different energy-transferring linkers (L = L^1, L^2, L^3, and L^4; Fig. 1a). To demonstrate their feasibility and benefits, Ir-L^3-Eu was conjugated with CD47 peptide GNYTCEVTELTREGETIIELK that can target signal regulatory protein alpha (SIRPα) overexpressed on immunocytes [19] for the visualization and quantification of SIRPα and its host cells (Fig. 1b). The SIRPα amount overexpressed on the immunocytes in blood samples quantified by ICP-MS provides an indication of the degree of immune response from different diseased people.

Fig. 1 Structures of the dual Ir-Eu tags linked by different linkers, L^1, L^2, L^3, and L^4, and their emission spectra under excitation at 400 nm (**a**). Ir-L^3-Eu-PEG-CD47-peptide for visualization of the SIRPα overexpressed on RAW264.7 macrophages at 475 nm (Ir) and 612 nm (Eu) under the excitation of 400 nm on LCSM and quantification by^{191}Ir and/or ^{193}Ir and ^{151}Eu and/or ^{153}Eu on ICP-MS (**b**)
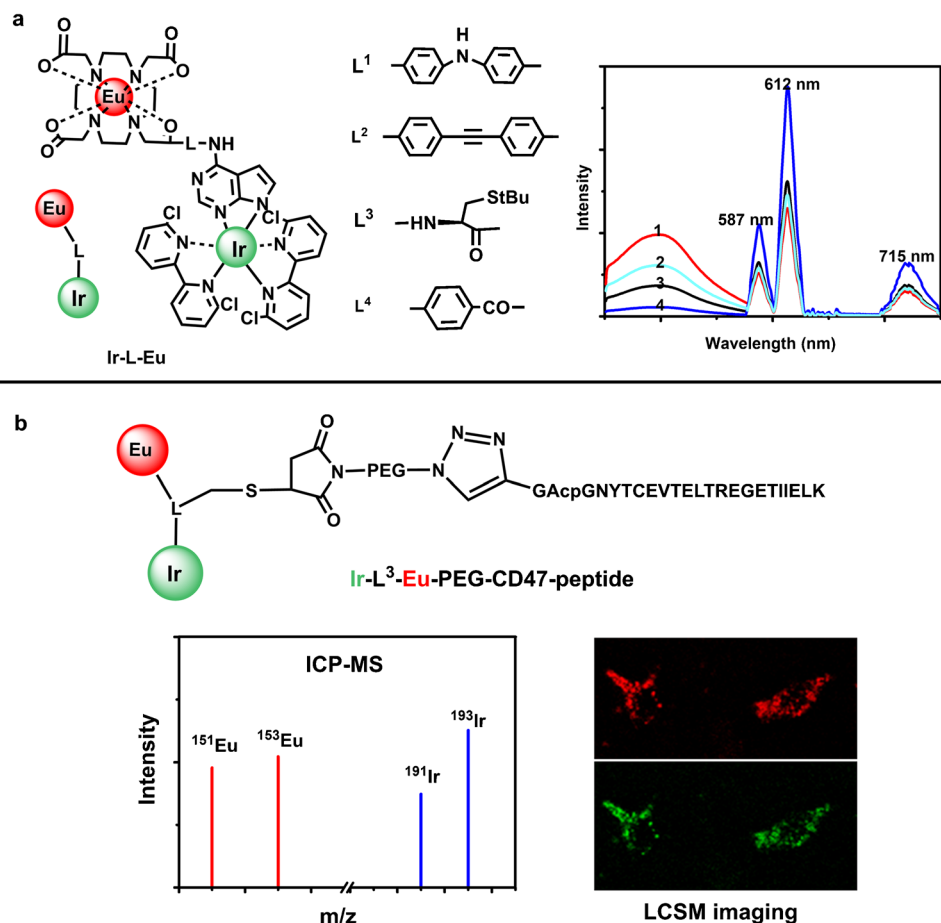
Materials and methods

Design and synthesis of the dual Ir-Eu tags and the CD47 peptide-conjugated Ir-L³-Eu for targeting SIRPα and its host cells

In order to obtain an Ir-Eu tag with effective fluorescent and ICP-MS signals, we started form the synthesis of DCBP-Ir-APP complex and then linked to Eu-DOTA with the linker molecules of bis(4-bromophenyl)amine (L^1), bis(4-bromophenyl) acetylene (L^2), N-(9-fluorenylmethoxycarbonyl)-s-tert-butylcystine (N-Fmoc-S-tBu-L-cystine, L^3), and 4-bromobenzoic acid (L^4) (Scheme S1-S2), respectively.

We first mixed $IrCl_3$ and DCBP in a solution of 2-ethoxyethanol:H_2O (3:1) and stirred the mixture for 8 h in room temperature and then heated to 125 °C and reflux for 48 h to obtain DCBP-Ir. Afterwards, APP was mixed with DCBP-Ir to obtain amino-modified Ir complex, DCBP-Ir-APP. L^1 was used to link DCBP-Ir-APP and DO3AtBu through the reaction between amino group and bromine to obtain Ir-L^1-Eu tag. Ir-L^2-Eu and Ir-L^4-Eu tags were synthesized via similar routes (Scheme S1 and see the detailed synthetic procedures, purification, and characterization in the Supplementary Material, Fig. S1-6).

To synthesize Ir-L^3-Eu tag, we used L^3 first to react with APP via the reaction between carboxyl and amino group to obtain a pyridine ligand containing the post reaction groups and then mixed with DCBP-Ir to obtain the DCBP-Ir-APP tag containing the amino group with Fmoc protection and the tBu-protected sulfhydryl group. After deprotecting the Fmoc from the amino group, and reacting with NHS-DOTA-Eu to obtain Ir-L^3-Eu-S-tBu. Subsequently, Mal-PEG (2000)-N_3 was used to react with the deprotected Ir-L^3-Eu-SH to obtain Ir-L^3-Eu-PEG-N_3. It was used to label alkynyl-CD47-peptide (GAcpGNYTCE-VTELTREGETIIELK) that targeted SIRPα via click reaction (Scheme S2 and see the detailed synthetic procedures, purification, and characterization in the Supplementary Material, Fig. S7-10).

LCSM imaging and ICP-MS quantification of SIRPα and its host cells

Macrophage cell line RAW264.7 (SIRPα-positive) and cervical carcinoma cell line Hela (SIRPα-negative), which were cultured in DMEM medium containing 10% FBS, 1% penicillin, and 1% streptomycin at 37 °C in a 5% CO_2 and 95% air incubator, were used to investigate the specificity of the Ir-Eu tags and alkynylated CD47-peptide towards the cells. Each kind of cells was seeded in a 12-well glass plate (1.0×10^4 cells per well) and incubated overnight. After washing with PBS buffer, added 20 µL 1 µM alkynylated CD47-peptide to each well and incubated for 3 h to label SIRPα on the surface of cells. After washing, 50 µL Ir-L^3-Eu-PEG-N_3, Ir-PEG-N_3, and Ir-L^3-Eu (1 µM each) as well as PBS buffer were added, respectively, and then 25

µL 10 µM $CuSO_4$, 27.5 µL 10 µM BIM, and 25 µL 100 µM sodium ascorbate were added and incubated for another 0.5 h for the click reaction between alkynylated CD47-peptide labeled and the azide group if available in the tags added. After washed five times using PBS buffer, the cells were first imaged on LCSM and then quantified using ICP-MS after dissolving the cells using an appropriate amount of ultrapure concentrated HNO_3 overnight and an appropriate dilution with ultrapure water. To further confirm the specificity towards SIRPα-positive cells, RAW264.7 cells were pre-incubated with 20 µL 1µM CD47 protein but not the alkynylated CD47-peptide for 3 h prior to the addition of 50 µL 1µM Ir-L^3-Eu-PEG-N_3 for a blocking experiment, while SIRPα-negative Hela cells were used as a control. Moreover, the SIPRα per cell in a series of known number RAW264.7 cells were quantified using ICP-MS. Based on this information obtained, in turn, number of the SIRPα-positive RAW264.7 cells can be counted.

We collected blood samples from the Affiliated Zhongshan Hospital of Xiamen University, including 27 blood samples from liver cancer patients, 26 cholecystitis, gastritis and pneumonia patients, and 12 lithiasis (detailed information is listed in Table S1). All the blood samples were stored at -80 °C until use. These obtained samples were approved by the hospital ethics committee, and the patients signed the informed consents (see the Supplementary Material). Prior to quantification of SIRPα and SIRPα-positive cells in blood using ICP-MS, the samples of 1 mL each were appropriately diluted with PBS buffer and incubated with the alkynylated CD47-peptide for 3 h followed by a click labeling with Ir-L^3-Eu-PEG-N_3 for 5 min and washing and centrifugation 5 times to get rid of the excess unreacted Ir-L^3-Eu-PEG-N_3 tag and alkynylated CD47-peptide.

Sources of the chemical and biochemical reagents used and instrumentation information were described in the Supplementary Material. Detailed synthesizing routes (Scheme S1-2) and conditions as well as their semi-preparative HPLC purification and fluorescence, NMR, and ESI-MS characterizations (Fig. S1-10) can be found in the Supplementary Material.

Results and discussion

Fluorescence and ICP-MS signals from the Ir-Eu tags

After ESI-TOF-MS and NMR characterizations of the designed and synthesized Ir-Eu tags, we evaluated their fluorescent and mass spectroscopic properties. DCBP-Ir-APP has an absorption spectrum from 310 to 420 nm and emits a corresponding fluorescent peak from 450 to 500 nm of 0.1 µs lifetime (τ_{Ir_0}) (Fig. S11a), which can match the energy level of Eu-DOTA. When DCBP-Ir-APP was linked to Eu-DOTA

via L^1, L^2, L^3, and L^4 of different molecular structure and excited at 400 nm, the emission intensity from DCBP-Ir-APP at 475 nm decreased along with the increase in emission intensity of Eu-DOTA at 591 nm ($^5D_0 \rightarrow {}^7F_1$), 612 nm ($^5D_0 \rightarrow {}^7F_2$), and 710 nm ($^5D_0 \rightarrow {}^7F_5$) (Fig. 1a and Fig. S11b). These phenomena observed confirmed the emission light from DCBP-Ir-APP can be absorbed by Eu-DOTA and profitably transferred the energy to Eu-DOTA. Theoretical calculation ($\eta = 1 - \tau_{Ir_i}/\tau_{Ir_0}$) according to the fluorescent lifetime (τ_{Ir_i}) determined at 475 nm [59 ns (L^1), 37 ns (L^2), 25 ns (L^3), and 18 ns (L^4)] of DCBP-Ir-APP linked to Eu-DOTA by the different linkers suggests that the energy transfer efficiency between DCBP-Ir-APP and Eu-DOTA, which is corresponding to the fluorescent efficiency, was 41% (L^1), 63% (L^2), 75% (L^3), and 82% (L^4). These results indicated that both length and structure of the linkers have significant impact on the fluorescent signals from Eu-DOTA in the Ir-Eu tags. In contrast to the fluorescent properties of the Ir-Eu tags, the ICP-MS signal intensities of ^{153}Eu and ^{193}Ir depend simply on their first ionization potential of Eu (5.67 eV) and Ir (8.97 eV) rather than the linkers (Fig. 1b), as we know that ICP is a very hard ionization source breaking the bonds between the atoms and making the atomic ions. When we use the Ir-Eu tags for ICP-MS application, the signals were not affected by the length and structure of the linkers. On the other hand, we must consider the possibility to conjugate a warhead into the tags for labeling the targeted bioanalytes. Regarding SIPRα and its host cells exemplified in this study, we selected Ir-L^3-Eu because it has a better fluorescent efficiency, more importantly, a tBu-protected -SH in Ir-L^3-Eu benefiting the chemical assembly of a post-conjugation moiety (MMA-PEG-N_3) as we desired for the labeling purpose (Fig. 1b). Subsequently, we further measured a series of Ir-L^3-Eu-PEG-N_3 solutions of different concentration from 0 to 500 nM to make a calibration curve at 612 nm (Fig. S12). The linear dynamic range was up to 200 nM, and the limit of detection (LOD, 3σ) was 6.3 pM with an RSD of 3.1% at 50 nM ($n = 3$). While the obtained ICP-MS results (Fig. S12) indicated that the LODs (3σ) when monitoring ^{153}Eu and ^{193}Ir were down to 0.4 and 0.8 pM, the linear dynamic range was up to 500 nM (higher concentrations were not tested) ($R^2 = 0.995$ and 0.997) with an RSD of 2.6% (^{153}Eu) and 3.1% (^{193}Ir) at 50 nM ($n = 5$). All these results suggested that although both fluorescence and ICP-MS signals could be obtained from the same Ir-L^3-Eu-PEG-N_3 tag, ICP-MS is superior to fluorescence from the viewpoint of analytical merits.

Specificity of Ir-L^3-Eu-CD47 peptide towards SIRPα and SIRPα-host cells

In our previous work, we found that SIRPα could be selectively labeled by CD47-peptide with a stoichiometry of 1:1 [20]. Here, we set SIPRα and its host cell as examples and used CD47-peptide to label SIRPα and then azido Ir-L^3-Eu-PEG-N_3 to conjugate the SIPRα-targeted alkynyl CD47-peptide through a click chemistry reaction to demonstrate their LCSM imaging and ICP-MS quantification. Prior to this, the fluorometric and ICP-MS analysis figures of SIRPα were tested. The obtained fluorometric results at 612 nm (Fig. S13) showed that the LOD (3σ) for SIRPα was 65.2 pM, and the linear dynamic range was from 0.07 to 100 nM ($R^2 = 0.920$) with an RSD of 3.2% at 50 nM ($n = 5$). While monitoring ^{153}Eu and ^{193}Ir on ICP-MS, the LOD was down to 0.5 and 1.1 pM SIRPα with a linear dynamic range up to 200 nM ($R^2 = 0.996$ and 0.997; higher concentrations were not tested) and an RSD of 2.6 and 3.2% at 50 nM ($n = 5$) (Fig. S13). The LOD of SIRPα using ICP-MS comparing to that of fluorometry is about 130 times lower, and the sensitivity remains almost unchanged as that of Ir-L^3-Eu-PEG-N_3 itself, indicating again the matrix-independent advantage of ICP-MS.

To further verify the targeting specificity of the alkynylated CD47-peptide towards the cells and the click labeling of Ir-L^3-Eu-PEG-N_3, we designed cell experiments using SIRPα-positive RAW264.7 macrophage as a model cell line and SIPRα-negative Hela cell line as a control. When we added alkynylated CD47-peptide into the cell culture and incubated for 3 h to target the SIRPα overexpressed on the cell surface, and then added Ir-L^3-Eu-PEG-N_3, Ir-PEG-N_3, and Ir-L^3-Eu tags, respectively, to label the SIRPα-targeted alkynylated CD47-peptide. The results obtained indicated that only RAW264.7 could be detected using ICP-MS monitoring ^{153}Eu and/or ^{193}Ir and visualized at 612 nm on LCSM in the cases of Ir-L^3-Eu-PEG-N_3 and 475 nm Ir-PEG-N_3 as expected, but not the cases of Ir-L^3-Eu and/or Hela cells (Fig. 2). Moreover, when the alkynylated CD47-peptide was not added or when RAW264.7 cells were pre-incubated with CD47 protein to block the SIRPα on RAW264.7, no fluorescent and ICP-MS signals from RAW264.7 could be detected. All these results obtained suggested that the specificity of alkynylated CD47-peptide towards the SIRPα-positive RAW264.7 cells and that of the click labeling reaction.

Subsequently, different known numbers of RAW264.7 cells were targeted first with alkynylated CD47-peptide and then labeled by Ir-L^3-Eu-PEG-N_3 for quantifying the amount of SIRPα overexpressed on per RAW264.7 cell using ICP-MS. The obtained results indicated that the average SIRPα overexpressed on each RAW264.7 cell was 4.71 ± 0.04 amol when 50,000 cells were employed ($n = 5$). Based on the LOD of SIRPα, down to 220 (^{153}Eu) and 830 (^{193}Ir) RAW264.7 cells could be directly counted using ICP-MS. It is worthy of mentioning that the ratio of ^{153}Eu/^{193}Ir remained constant even though the SIRPα concentration and/or the cell number increased (Fig. 3a and Fig. S14), which implying that it can serves as a precision control of the labeling process, allowing internal validation of the quantitative results obtained.
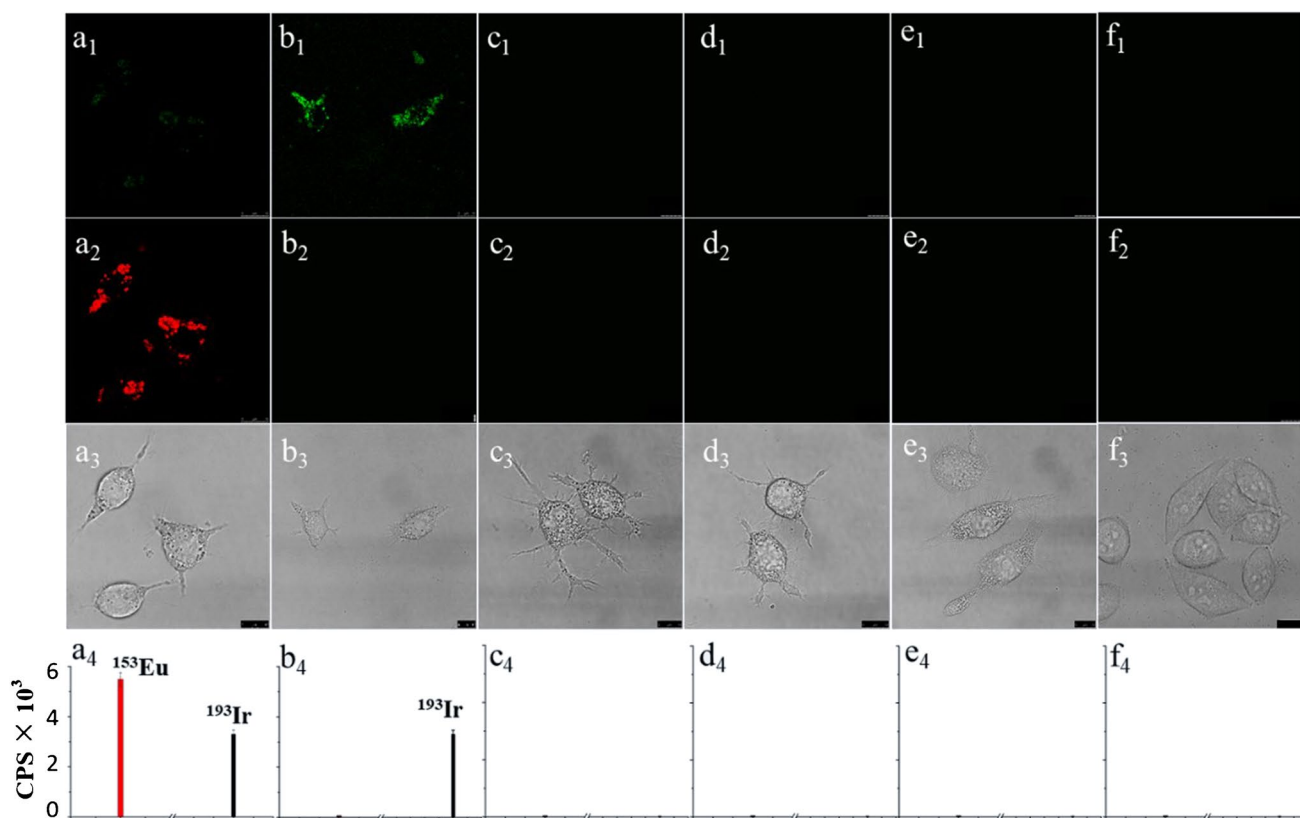
Fig. 2 LCSM images of SIRPα on the surface of RAW264.7 incubated first with alkynylated CD47-peptide and then labeled with Ir-L^3-Eu-PEG-N$_3$ (a$_1$–a$_4$), Ir-PEG-N$_3$ (b$_1$–b$_4$), and Ir-L^3-Eu (c$_1$–c$_4$); RAW264.7 without alkynylated CD47-peptide incubation and labeled directly with Ir-L^3-Eu-PEG-N$_3$ (d$_1$–d$_4$); RAW264.7 pre-incubated with CD47 protein to block SIRPα on the surface of the cells and then incubated with alkynylated CD47-peptide and labeled by Ir-L^3-Eu-PEG-N$_3$ (e$_1$–e$_4$); SIRPα-negative Hela cells were used as a control (f$_1$–f$_4$)
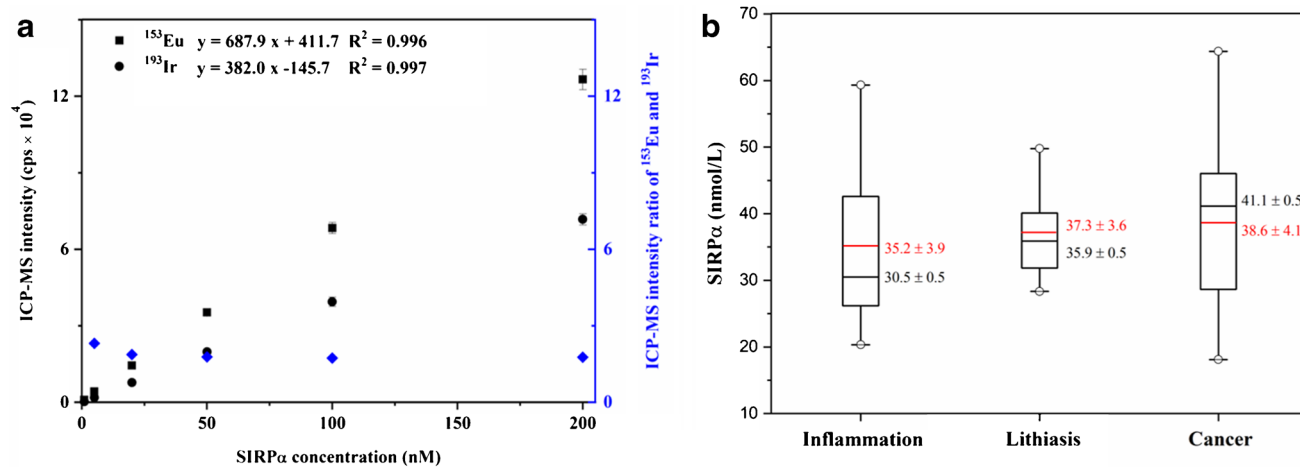
Fig. 3 Calibration curves of SIRPα concentration against ICP-MS intensities of ^{153}Eu and ^{193}Ir labeled as well as their ratio (**a**); box-plots of SIRPα concentrations in the blood samples from the patients of liver cancer ($n = 27$), lithiasis ($n = 12$), and inflammation ($n = 26$). The boxes represent the 25th and 75th percentiles, the whiskers represent the 5th and 95th percentiles, and outliers are displayed by circles. The black lines represent the median value; the red lines represent the mean value (**b**)

Quantification of SIRPα and estimation of SIPRα-host immunocytes in real blood samples using ICP-MS After verifying the specificity of alkynylated CD47-peptide towards SIRPα and its host cells as well as the click-labeling of $Ir-L^3$-Eu-PEG-N_3, SIRPα in real blood samples were quantified using ICP-MS. The obtained results (Fig. 3b and Table S1) showed that the SIRPα quantified in liver cancer blood samples ranged from 18.1 ± 0.2 to 64.4 ± 1.6 μmol/mL with the mean and median values of 38.6 ± 4.1 μmol/mL and 41.1 ± 0.5 μmol/mL ($n = 27$). When further analyzing these data in details, we could see that the mean and median concentrations of the SIRPα in liver cancer blood samples are the biggest, following by 37.3 ± 3.6 μmol/mL (mean) and 35.9 ± 0.5 μmol/nL (median) from 28.3 ± 0.1 to 49.8 ± 0.8 μmol/mL in the lithiasis blood samples ($n = 12$) and 35.2 ± 3.9 μmol/mL (mean) and 30.5 ± 0.5 μmol/mL (median) from 20.3 ± 0.2 to 59.3 ± 1.3 μmol/mL in the inflammation blood samples ($n = 26$). It should be noted that the SIRPα-positive cells in blood sample are not limited to macrophage (for example, RAW264.7 demonstrated here), but also include monocyte, dendritic cell, neutrophil, eosinophil, and basophilic granulocyte, which are all immunocytes. If we might roughly estimate the SIRPα-host immunocyte number that may reflect the degree of immune response of the patients based on the average content of SIRPα on each RAW264.7, the SIRPα-host cell number ranged from 3.84 ± 0.04 to $13.67 \pm 0.33 \times 10^6$ with $8.20 \pm 0.86 \times 10^6$ (mean) and $8.73 \pm 0.16 \times 10^6$ (median) in the liver cancer blood samples, 6.02 ± 0.02 to $10.57 \pm 0.16 \times 10^6$ with $7.91 \pm 0.76 \times 10^6$ (mean) and $7.62 \pm 0.10 \times 10^6$ (median) in the lithiasis blood samples and 4.32 ± 0.02 to $12.59 \pm 0.28 \times 10^6$ with $7.46 \pm 0.82 \times 10^6$ (mean) and $6.47 \pm 0.11 \times 10^6$ (median) in the inflammation blood samples (Table S1). Clearly, although the diagnostic meaning behind these data presented here needs further investigation together with professionally medical doctors in the future when considering individual differences even among patients with the same disease, the design of a dual-element Ir-Eu tag did provide an alternatively selectable way for biomarkers quantification and cells counting using ICP-MS, which allowing internal validation of the quantitative results obtained.

Conclusions

We designed and synthesized a dual Ir-Eu tag that offers both fluorescence and ICP-MS signals for bioanalysis, enabling the imaging and quantification of a biomarker and its host cells. Although the LOD using the dual Ir-Eu tag is similar to that of our previous work [6], the two different ICP-MS detectable Ir and Eu are available for the internal validation of the quantitative results obtained. Such an idea is not limited to the analysis of SIPRα and its host cells exemplified here; we envision that more applications to bioanalysis could be expected when more dual-element and even multi-element tags are designed and prepared towards targeting more biomarkers and their host cells in the future. On the other hand, we believe that the individual SIPRα-host immunocytes, rather than a little bit rough estimation of their total numbers in the blood samples demonstrated here, will be recognized and counted on a single-cell multi-parameter ICP-MS platform as the development of the Ln-encoded signal-amplification strategies [21–25], in which not only dual- but also multi-element tags will play a unique role.

Declarations

References

1. Liu R, Zhang SX, Wei C, Xing Z, Zhang SC, Zhang XR. Metal stable isotope tagging: renaissance of radioimmunoassay for multiplex and absolute quantification of biomolecules. Acc Chem Res. 2016;49:775–83.
2. Sanz-Medel A, Montes-Bayón M, Bettmer J, Fernández-Sanchez ML, Encinar JR. ICP-MS for absolute quantification of proteins for heteroatom-tagged, targeted proteomics. Trac-Trends Anal Chem. 2012;40:52–63.
3. Yan XW, Yang LM, Wang QQ. Detection and quantification of proteins and cells by use of elemental mass spectrometry: progress and challenges. Anal Bioanal Chem. 2013;405:5663–70.
4. Liang Y, Yang LM, Wang LM. An ongoing path of element-labeling/tagging strategies toward quantitative bioanalysis using ICP-MS. Appl Spectrosc Rev. 2016;51:117–28.
5. Liang Y, Jiang X, Yuan R, Zhou Y, Ji CX, Yang LM, Chen HF, Wang QQ. Metabolism-based click-mediated platform for specific imaging and quantification of cell surface sialic acids. Anal Chem. 2017;89:538–43.
6. Liu CL, Lu S, Yang LM, Chen PJ, Bai PM, Wang QQ. Near-infrared neodymium tag for quantifying targeted biomarker and counting its host circulating tumor cells. Anal Chem. 2017;89:9239–46.

7. Zhang ZB, Yan XW, Xu M, Yang LM, Wang QQ. A dual-labelling strategy for integrated ICPMS and LIF for the determination of peptides. J Anal At Spectrom. 2011;26:1175–7.

8. Zhang ZB, Luo Q, Yan XW, Li ZX, Luo YC, Yang LM, Zhang B, Chen HF, Wang QQ. Integrin-targeted trifunctional probe for cancer cells: a "seeing and counting" approach. Anal Chem. 2012;84:8946–51.

9. Liang Y, Jiang X, Tang NN, Yang LM, Chen HF, Wang QQ. Quantification and visualization of glutathione S-transferase omega 1 in cells using inductively coupled plasma mass spectrometry (ICP-MS) and fluorescence microscopy. Anal Bioanal Chem. 2015;407:2373–81.

10. Yuan JL, Wang GL. Lanthanide complex-based fluorescence label for time-resolved fluorescence bioassay. J Fluoresc. 2005;15:559–68.

11. Bünzli JCG. Lanthanide Luminescence for Biomedical Analyses and Imaging. Chem Rev. 2010;110:2729–55.

12. Yan XW, Yang LM, Wang QQ. Lanthanide-coded protease-specific peptide-nanoparticle probes for a label-free multiplex protease assay using element mass spectrometry: a proof-of-concept study. Angew Chem Int Ed. 2011;50:5130–3.

13. Schwarz G, Mueller L, Beck S, Linscheid MW. J Anal At Spectrom. 2014;29:221–33.

14. Wendt K, Gottwald T, Mattolat C, Raeder S. Ionization potentials of the lanthanides and actinides-towards atomic spectroscopy of super-heavy elements. Hyperfine Interact. 2014;227:55–67.

15. Chen FF, Chen ZQ, Bian ZQ, Huang CH. Sensitized luminescence from lanthanides in d–f bimetallic complexes. Coord Chem Rev. 2010;254:991–1010.

16. Xu LJ, Xu GT, Chen ZN. Recent advances in lanthanide luminescence with metal-organic chromophores as sensitizers. Coord Chem Rev. 2014;273–274:47–62.

17. Lian P, Wei HB, Zheng C, Nie YF, Bian J, Bian ZQ, Huang CH. Synthesis, characteristics and photoluminescent properties of novel Ir-Eu heteronuclear complexes containing 2-carboxyl-pyrimidine as a bridging ligand. Dalton Trans. 2011;40:5476–82.

18. Sykes D, Cankut AJ, Ali NM, Stephenson A, Spall SJP, Parker SC, Weinstein JA, Ward MD. Sensitisation of Eu(III)-and Tb(III)-based luminescence by Ir(III) units in Ir/lanthanide dyads: evidence for parallel energy-transfer and electron-transfer based mechanisms. Dalton Trans. 2014;43:6414–28.

19. Rodriguez PL, Harada T, Christian DA, Pantano DA, Tsai RK, Discher DE. Minimal "self" peptides that inhibit phagocytic clearance and enhance delivery of nanoparticles. Science. 2013;339:971–5.

20. Liu CL, Yu DX, Ge FC, Yang LM, Wang QQ. Fluorescent and mass spectrometric evaluation of the phagocytic internalization of a CD47-peptide modified drug-nanocarrier. Anal Bioanal Chem. 2019;411:4193–202.

21. Yuan R, Ge FC, Liang Y, Zhou Y, Yang LM, Wang QQ. Virus-like element-tagged nanoparticle inductively coupled plasma mass spectrometry signal multiplier: membrane biomarker mediated cell counting. Anal Chem. 2019;91(4948–52):21.

22. Liang Y, Liu Q, Zhou Y, Chen S, Yang LM, Zhu M, Wang QQ. Counting and recognizing single bacterial cells by a lanthanide-encoding inductively coupled plasma mass spectrometric approach. Anal Chem. 2019;91:8341–9.

23. Zhou Y, Chen ZQ, Zeng JX, Zhang JX, Yu DX, Zhang B, Yan XW, Yang LM, Wang QQ. Direct infusion ICP-qMS of lined-up single-cell using an oil-free passive microfluidic system. Anal Chem. 2020;92:5286–93.

24. Liu Z, Liang Y, Zhou Y, Ge FC, Yan XW, Yang LM, Wang QQ. Single-cell fucosylation breakdown: switching fucose to europium. iScience 2021;24:102397.

25. Resano M, Aramendia M, Garcia-Ruiz E, Bazo A, Bolea-Fernandez E, Vanhaecke F. Living in a transient world: ICP-MS reinvented via time-resolved analysis for monitoring single events. Chem Sci. 2022;13:4436–73.